Lab on a Chip

PAPER

View Article Online
View Journal | View Issue

Cite this: *Lab Chip*, 2014, **14**, 2437

Preparation of monodisperse microbubbles using an integrated embedded capillary T-junction with electrohydrodynamic focusing†

Maryam Parhizkar,[a] Eleanor Stride[ab] and Mohan Edirisinghe*[a]

Received 15th March 2014,
Accepted 30th April 2014

DOI: 10.1039/c4lc00328d

www.rsc.org/loc

This work investigates the generation of monodisperse microbubbles using a microfluidic setup combined with electrohydrodynamic processing. A basic T-junction microfluidic device was modified by applying an electrical potential difference across the outlet channel. A model glycerol air system was selected for the experiments. In order to investigate the influence of the electric field strength on bubble formation, the applied voltage was increased systematically up to 21 kV. The effect of solution viscosity and electrical conductivity was also investigated. It was found that with increasing electrical potential difference, the size of the microbubbles reduced to ~25% of the capillary diameter whilst their size distribution remained narrow (polydispersity index ~1%). A critical value of 12 kV was found above which no further significant reduction in the size of the microbubbles was observed. The findings suggest that the size of the bubbles formed in the T-junction (*i.e.* in the absence of the electric field) is strongly influenced by the viscosity of the solution. The eventual size of bubbles produced by the composite device, however, was only weakly dependent upon viscosity. Further experiments, in which the solution electrical conductivity was varied by the addition of a salt indicated that this had a much stronger influence upon bubble size.

Introduction

Over the past decade several techniques have been developed to generate microbubbles. Amongst these techniques, sonication and fractionation,[1] electrohydrodynamic atomization[2,3] and microfluidic devices[4,5] are the most commonly used. Generation of microbubbles with diameters smaller than 10 μm from electrified cone jets using the electohydrodynamic atomization (EHDA) technique was reported by Farook *et al.*,[3] where the jet breakup and microbubbling zones were thoroughly investigated. Whilst much narrower than those obtained by sonication, the microbubble size distributions obtained with this method were not perfectly monodisperse. Microfluidic devices on the other hand offer an unparalleled level of control over microbubble size and size distribution,[6–9] facilitating the formation of microbubbles suitable for a diverse range of applications, including in the biomedical field.[10,11] One disadvantage of using microfluidics for preparing bubbles in the <10 μm range, however, is the tendency for microchannels to become clogged.[12,13]

Fluid flow in the channels of microfluidic devices has most commonly been controlled using high precision mechanical pumps.[14] However, another type of flow in microchannels, broadly refrered to as electroosmotic flow,[15] initiated by the application of an electric field, has also been studied extensively.[16] This method of driving and controlling the operating fluid, has some distinct advantages due to the localization of the electrical forces in these miniaturized devices. High electric fields can be obtained with relative ease and they can assist with the flow of fluids in the microchannels.[17] Thus, in order to alleviate the difficulties of excessive pressure gradients associated with microfluidic pumps in microchannels, pressure driven flows are often replaced by electroosmotic flows.[18]

Electrically driven microfluidic devices have previously been used in many studies for mixing of two phase flows,[19] and generation of monodisperse droplets,[20–22] fibers[23,24] and microbubbles.[25] Kim *et al.*[20] developed a microchip droplet generator using an electrohydrodynamic actuation method. Droplet formation was controlled by the application of an electric field between the charged liquid sample and a ground electrode without the need for an external pneumatic pump. Srivastava and coworkers[24] described a microfluidic based electrospinning method to fabricate hollow and core/sheath

[a] *Department of Mechanical Engineering, University College London, Torrington Place, London, WC1E 7JE, UK. E-mail: m.edirisinghe@ucl.ac.uk; Fax: +44 (0)2073880180; Tel: +44 (0)2076793942*
[b] *Institute of Biomedical Engineering, Department of Engineering Science, University of Oxford, Old Road Campus Research Building, Headington, Oxford OX3 7DQ, UK*

† Electronic supplementary information (ESI) available. See DOI: 10.1039/c4lc00328d

nanofibers. Of particular relevance to the present study, Pancholi *et al.*[25] produced phospholipid coated microbubbles with diameters smaller than 8 μm using a device consisting of a combined T-junction microfluidic and electrospraying device. However, the size distibution of microbubbles produced in this study was still relatively broad.

Using a T-junction microfluidic device is one of the easiest methods of producing highly monodisperse microbubbles. However, to generate bubbles with diameters smaller than the geometrical diameter of the channels, using mechanically assembled devices is challenging due to constraints on capillary size, especially at higher viscosities.[26] As indicated above, the use of an electric field can offer significant advantages for liquid manipulation in microchannels. The small channel cross sectional area presents high electrical resistance to ionic currents, which allows high electric fields to be maintained with low currents and hence provides control over the liquid velocity.[27] This in turn provides control over the breakup of the gas column and formation of bubbles. While microfluidics and EHD have been separately used to produce microbubbles, to the best of the authors' knowledge, the direct combination of these two methods to form monodisperse bubbles has not been reported in the literature. The capillary embedded T-junction device described in this work provides a simple but yet robust means of producing highly monodisperse microbubbles. However, because the channel diameters are relatively large (compared with *e.g.* devices prepared *via* photolithography) the production of bubbles that are signfiicantly smaller than the channel diameter is not viable with purely mechanically driven flow. In this work, we present a microfluidic system with integrated electrohydrodynamic focusing with the aim of both reducing bubble size and maintaining monodispersity. We investigate the effect of applied voltage, solution viscosity and electrical conductivity on the production of microbubbles and their characteristics. We show that by introducing an electric field directly into the bubble break up region, the flow of the continuous phase is assisted by electrohydrodynamic forces and bubbles with almost an order of magnitude smaller than the channel diameter can be generated.

Materials and methods

Materials

Glycerol–water mixtures with viscosities ranging from 1.3 to 36 mPa s were used as the continuous liquid phase. Glycerol with 99% purity (Sigma Aldrich, U.K.) was diluted with distilled water to generate the concentrations shown in Table 1. In order to facilitate bubble formation and reduce the surface tension to stabilize newly created interfaces, an equal amount of 0.01 M SLS (Sodium Lauryl Sulfate, VWR, UK) solution was added to all the solutions. In order to investigate the effect of liquid electrical conductivity, 1 wt.% sodium chloride solution (NaCl, Sigma Aldrich, U.K.) was also added to a solution of 50 wt.% glycerol concentration to increase the conductivity while keeping the viscosity and surface tension constant. Air was used as the dispersed (gas) phase throughout the study.

Characterization of solutions

The density of all the solutions used in the experiments was measured using a DIN ISO 3507- Gay-Lussac type standard density bottle. Surface tension for each solution was measured using a Drop Shape Analysis System, Model DSA100 (Kruss GmbH, Hamburg, Germany) using the plate method. Viscosity was measured using a Brookfield DV-11 Ultra programmable Rheometer (Brookfield Engineering Laboratory Inc., USA). Electrical conductivity and pH were measured using a Bench pH/mV/EC/TDS/NaCl combination meter (Hanna Instruments Ltd, UK). All the measurements, presented in Table 1, were performed at the ambient temperature (22 °C) after calibrating the equipment using distilled water.

Experimental setup

The experimental setup consisted of two Teflon FEP (Fluorinated Ethylene Polypropylene) capillaries with outer diameter of 1.58 mm inserted perpendicularly into a Polydimethylsiloxane (PDMS) block (100 × 100 × 10 mm) as inlet channels for the gas and liquid flows. A third stainless steel capillary was embedded in the polymer block co-axially aligned with the gas inlet channel with a 200 μm distance to create the junction where the two phases meet. The internal diameter for all of the channels was fixed at D_{ch} = 100 μm. A schematic of the T-junction set up is shown in Fig. 1. The top capillary was connected to a gas regulator fitted to a pressurized air tank *via* a 6 mm diameter tube, where the gas was supplied to the junction at constant pressure P_g. A digital manometer was connected to the tube to measure the in-line gas pressure. Also a gas regulator was used to vary the pressure supplied to the T-junction. The capillary supplying the liquid phase was connected to a 20 ml stainless steel syringe (KD Scientific, Holliston, MA, USA). A Harvard syringe pump PHD-4400 (Harvard Apparatus Ltd., Edenbridge, UK) was used to flow liquid through the capillaries at a constant flow rate. To apply an electrical potential difference across the device, the steel capillary tube was connected to a high

Table 1 Characteristic properties of solutions used in the experiments

Aqueous solution	Viscosity (μ/mPa s)	Surface tension (σ/mN m^{-1})	Electrical conductivity (k/μS cm^{-1})	pH
5 wt.% glycerol, 1 wt.% SLS	1.3	50	120	4.8
50 wt.% glycerol, 1 wt.% SLS	6	56	18	8.2
50 wt.% glycerol, 1 wt.% SLS, 1 wt.% NaCl	6	56	1500	7.4
65 wt.% glycerol, 1 wt.% SLS	15	57	16	8.3
75 wt.% glycerol, 1 wt.% SLS	36	59	14	8.4

voltage power supply (Glassman Europe Ltd. Tadley, UK) while the ground electrode was placed 100 mm below the tip of the outlet channel. For a solution with a given viscosity and liquid flow rate, monodisperse bubble formation occurs for a range of gas pressures with the smallest bubble size obtained at the lowest gas pressure and largest bubble size at the highest gas pressure. In this experimental investigation, the lowest gas pressure at which monodisperse bubble formation was achievable, was identified and used for each solution. Once the gas pressure and liquid flow rates required for stable bubble formation in the T-junction were determined, the applied voltage across the outer steel tube was varied between 6 and 21 kV.

Bubble characterization

Bubbles were collected from the outlet of the device on microscope slides and immediately observed under an optical microscope (Nikon Eclipse ME 600) fitted with a camera (JVC KY-F55B). Bubbles were studied at 5×, 10× and 20× magnification. For each sample/time point, 20 bubbles were chosen at random to measure the diameter and stability over a fixed collection area of 1.5 mm^2. A Phantom V7.3 high speed camera with a maximum resolution of 800 × 600 pixels at up to 4800 fps giving 1.2 seconds of recording time (Vision Research Ltd. Bedford, U.K.) was also used to obtain real time video images of the bubble formation process.

Theoretical description

Prior to considering the action of an electric field on the formation of microbubbles, it is beneficial to introduce the key dimensionless parameters characterizing the system, to determine the relative importance of the different parameters and forces involved, namely:

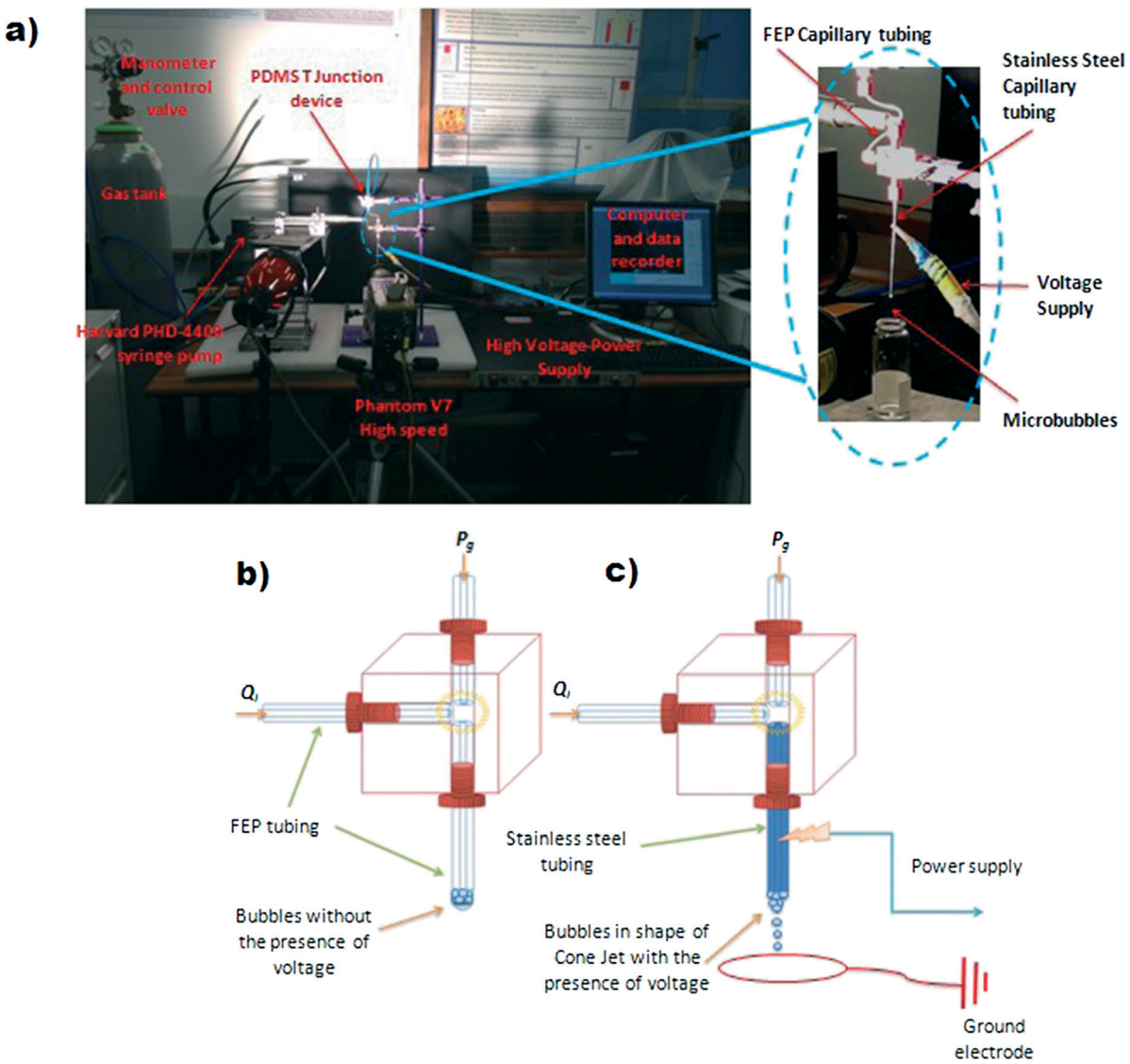

Fig. 1 T-junction setup a) and schematic of the T-junction setup and bubble formation without b) and with c) an applied electric field.

$$\mathrm{Re_l} = \rho_l U_l/\mu_l$$

$$\mathrm{Ca} = \mu_l U_l/\sigma_l$$

Where, $\mathrm{Re_l}$ and Ca refer to the Reynolds and Capillary number and μ_l, U_l, σ_l and ρ_l, are the liquid viscosity, velocity, surface tension and density, respectively. Re represents the ratio of the inertial to viscous forces and Ca represents the ratio of viscous forces and surface tension acting on an interface. For the liquid phase $7 \times 10^{-5} \leq \mathrm{Re_l} \leq 9.3 \times 10^{-3}$. When $\mathrm{Re_l} < 1$ flow is dominated by viscous stresses and pressure gradients and therefore inertial effects are negligible. According to electrohydrodynamic theory,[28,29] the electric Korteweg–Helmholtz force exerted per unit volume of fluid can be written as:

$$f_e = \rho_e \bar{E} - \frac{1}{2}\bar{E}^2 \nabla \varepsilon_l + \frac{1}{2}\nabla\left(\bar{E}^2 \frac{d\varepsilon_l}{d\rho}\rho\right) \quad (1)$$

Where ρ_e is the volume charge density, ρ is the liquid density, ε is the dielectric constant for the liquid and $\bar{E}$ is the electric field strength. The first term on the right hand side of eqn (1) represents the Coulomb force acting on the free charge and can be neglected when the current is small. The second term is the dielectrophoresis force exerted on the liquid due to the spatial gradient in the permittivity,[30] which is classified as the main force acting on the liquid–gas interface. For a spherical bubble:

$$F_{DEP} = \frac{2\pi D_b^3 \varepsilon_l (\varepsilon_g - \varepsilon_l)}{\varepsilon_g + 2\varepsilon_l} \nabla \bar{E}^2 \quad (2)$$

Where D_b is the bubble diameter. Since the dielectric constant of a gas is smaller than that of a liquid, F_{DEP} at the liquid–gas interface will act towards the centre of the bubble. In the presence of the electric field, a bubble emerging into the outlet channel becomes polarized and when the electric field is applied, the bubble moves away from the contact area. By varying the pressure distribution in the liquid phase, this force increases the elongation of the gas column into the outlet channel. The third term in eqn (1) refers to the electrostriction force which is negligible in this case due to the minimal influence of fluid compressibility on bubble formation.

In the absence of an electric field, the competition between liquid and gas pressure, viscous forces and interfacial tension controls the breakup of the gas column into bubbles. Once the sum of the viscous stress and pressure difference due to the obstruction of channel by the emerging gas column exceeds the capillary pressure, detachment begins. The capillary force F_σ is given by the difference between the Laplace pressures upstream and downstream of the emerging bubble multiplied by the projected area of the emerging interface (where R_1 and R_2 are the radii of curvature axially and radially and $A_{interface}$ is the projected area).

$$F_\sigma \approx \sigma\left(\frac{1}{R_1} + \frac{1}{R_2}\right) A_{interface} \quad (3)$$

The viscous shear force F_τ is given by the product of viscous stress acting on the emerging interface and the projected area of the emerging interface.

$$F_\tau \approx \mu_l Q_l A_{interface} \quad (4)$$

Finally, following Garstecki *et al.*[31] the squeezing pressure force:

$$F_p \approx \Delta P_c A_{interface} \quad (5)$$

When an electric field is applied, electrical charge accumulates at the gas liquid interface which behaves as a capacitor. As the voltage increases, the charge build up at the interface increases resulting in an additional force on the gas column. The resulting elongation of the gas column in the axial direction and radial compression accelerates the breakup process and therefore leads to smaller bubbles.

Results and discussion

Influence of electric field on bubble formation

As above, once the flows of the two phases in the junction reach equilibrium, bubbles are formed whose size depends upon the balance of capillary pressure, Laplace pressure and liquid shear stress.[32] For these experiments the solution viscosity was fixed and the flow rate and the minimum gas pressure required to produce the smallest bubble size, for a fixed polydispersity index was determined. In the absence of an electric field a hemispherical droplet containing microbubbles was observed emerging from the tip of the outlet capillary (Fig. 2a). This shape is due to liquid surface tension exceeding the weight of the droplet. With the application of an electrical potential difference, the air–liquid interface became polarized causing deformation of the meniscus containing bubbles (Fig. 2b). With increasing voltage the droplet adopted a conical shape (Fig. 2c), referred to as a "Taylor" cone.[33] With increasing voltage, the surface tension cannot maintain the liquid

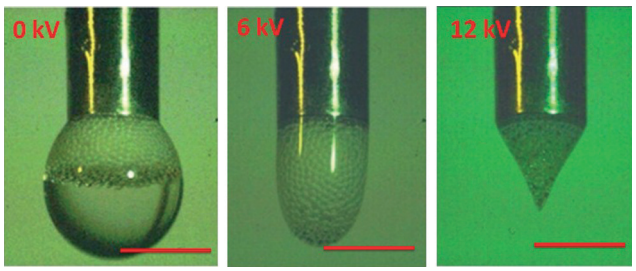

Fig. 2 High speed camera images of microbubbles at the tip of the outlet for 50 wt% glycerol solution at applied voltages of 0, 6 and 12 kV. Scale bar is 1.6 mm.

inside the meniscus, thus a thin jet at tip of the cone appears containing smaller microbubbles, which subsequently breaks up into a spray. In this set up the formation of a "Taylor" cone and stable jet was initiated at 9 kV.

As well this observable effect at the tip of the outlet channel, as above, a tangential electrical force is created that leads to faster breakup of the gas column at the junction, therefore reducing the detachment time and leading to the formation of smaller bubbles at a faster rate.[34]

Effect of voltage increment on microbubble size

Bubble formation under the influence of an electric field was observed in the experiments using aqueous glycerol solution with 5, 50, 65 and 75 wt% glycerol concentrations in order to determine the effect of viscosity. The liquid flow rate was set for all the experiments as 0.01 ml min^{-1}, while the gas pressure was adjusted to generate monodisperse bubbles for each solution.

Once the bubbles were formed at the minimum gas pressure (P_{gmin}) for each solution, the applied voltage was increased to 6 kV, where the meniscus at the tip of the outlet channel became thinner while the jet diameter was reduced and therefore microbubble size decreased. For instance, for the lowest solution viscosity (1.3 mPa s) the diameter of microbubbles produced without an electric field was 170 μm, which reduced to 120 μm at 6 kV (Fig. 3). By increasing the voltage to 9 kV, a cone jet was created at the tip of the outlet channel and the size of bubbles reduced further, to 40 μm with a polydispersity index (PDI, defined as the ratio between the standard deviation and mean diameter in percentage) of ~1%. At 12 kV, the cone jet broke up into a spray of fine liquid threads and bubbles with even smaller diameters (30 ± 0.95 μm) were produced.

This process was repeated for solutions with higher glycerol concentration and viscosities of 6, 15 and 36 mPa s and it was shown that increasing the voltage also affected bubble size for the highest viscosity solution while the smallest microbubble diameter of 25 μm was produced for the solution with 36 mPa s viscosity at 12 kV.

Increasing the applied voltage to 15 kV, did not change the bubble size significantly at any of the glycerol concentrations. However bubble stability decreased, most likely as a result of coalescence due to the higher surface charge. Fig. 4 shows microscopic images of microbubbles produced from 75% glycerol solution at constant liquid flow rate and applied voltages of 12–21 kV. It is evident from the images that at 12

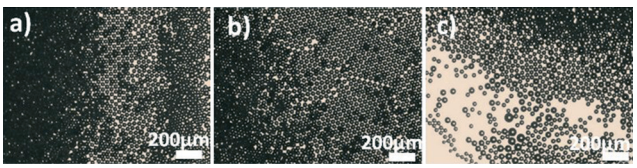

Fig. 4 Optical micrographs of microbubbles from a solution with 75% glycerol concentration at constant liquid flow rate of 0.01 ml min^{-1} at applied voltages of a) 12, b) 15 and c) 21 kV.

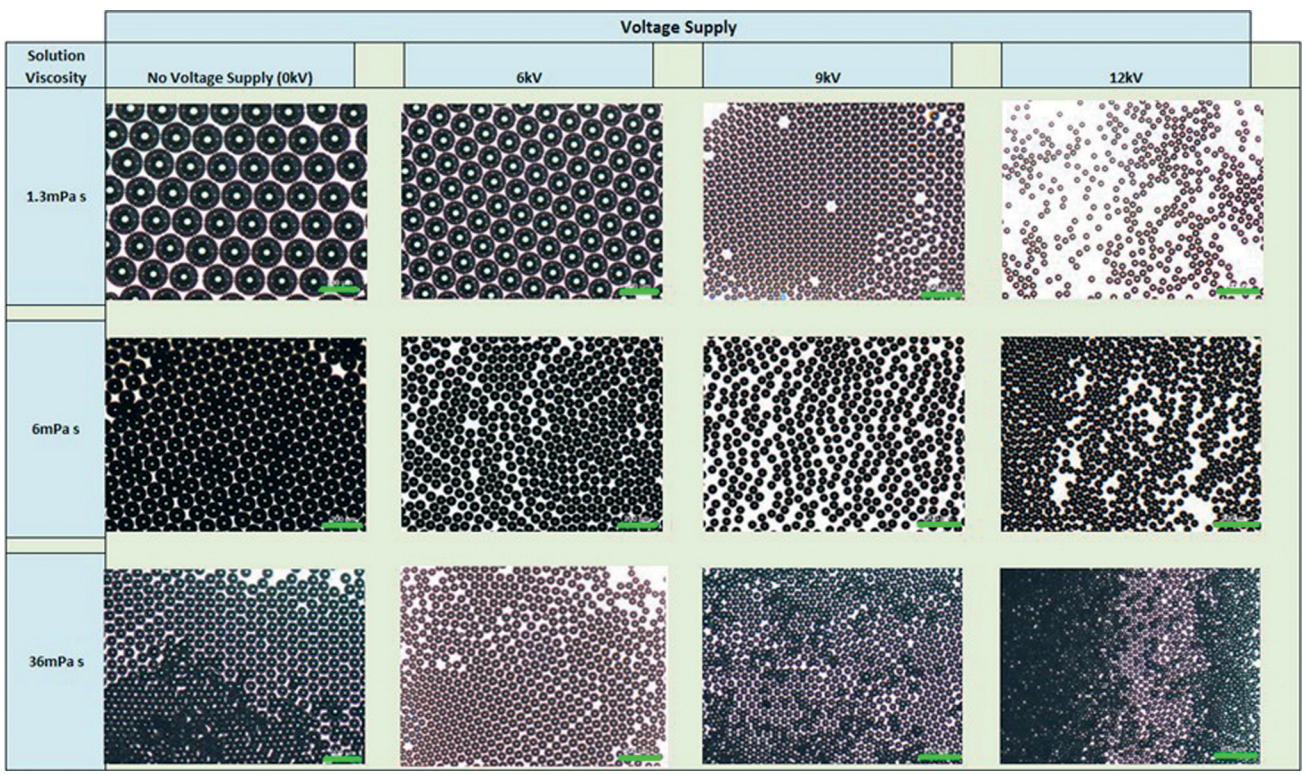

Fig. 3 Optical micrographs of bubbles formed in aqueous glycerol solutions with 5, 50 and 75% concentration at applied voltages of 0, 6, 9 to 12 kV and a constant liquid flow rate of 0.01 ml min^{-1}. Scale bar is 200 μm.

and 15 kV the bubble size was the same (25 μm) and they were near monodisperse.

However, increasing the voltage supply to 21 kV led to a much broader size distribution. This suggests that the optimum voltage for this system is 12 kV and increasing the voltage above this rate only reduces microbubble stability and monodispersity. A series of graphs were plotted (Fig. 5) to show the variation in microbubble size with increasing voltage. In all cases, as the voltage increased bubble diameter decreased; however a dramatic decrease in bubble diameter was observed between 6–9 kV for the solution with lowest viscosity that was not seen in the other solutions (Fig. 5a). This is most likely to be due to the fact that the solution with 5% glycerol concentration has a much higher dielectric constant[35] and therefore the effect of applied voltage on bubble diameter is greater. The scaling law proposed by Pantano *et al.*[36] predicts that the diameter of droplets produced by electrospraying is inversely proportional to the liquid dielectric constant.

In order to investigate the effect of viscosity, surface tension, flow rate ratio and applied voltage supply in parallel, a 3D plot of the variation of ratio of bubble diameter to channel width was plotted as shown in Fig. 5b. It can be observed that for each value of the capillary number, with increasing voltage the bubble to channel diameter ratio decreased dramatically between 0 and 9 kV. The reduction in this value is less significant, however at larger voltages. According to Ku and Kim,[37] for highly conducting and viscous liquids, the size of droplets electrosprayed from a "Taylor" cone are found to be relatively insensitive to the applied voltage and as long as the corona discharge density is not too high, monodisperse droplets are produced. Corona discharge is caused by the ionization of the surrounding medium that occurs once the electric field strength exceeds a certain level (the corona threshold voltage) while conditions are inadequate for a complete electrical breakdown. Above this voltage, there is a limited region, in which current increases proportionately with voltage according to Ohm's law. After this region, the current increases more rapidly, leading to complete breakdown and arcing or sparking at a point called the breakdown potential. It is also shown in Fig. 5b that with increasing capillary number, there is a smaller reduction in bubble size for the same increase in applied voltage. This suggested that there other parameters such as solution electrical conductivity and relative permittivity as mentioned previously that influence the bubble formation process. To investigate this further, NaCl was added to the solution keeping the concentration of glycerol constant at 50% in order to increase the electrical conductivity while keeping the other solution parameters constant. The results are plotted in Fig. 6 and as predicted, by increasing the electrical conductivity of the solution while keeping the viscosity and flow ratio constant, the influence of the voltage supply on microbubble size increases. This explains the dramatic decrease in bubble diameter in the graph representing the solution with lowest concentration of glycerol compared with the other graphs in Fig. 5. The electrical conductivity of the liquid phase is one of the key parameters in determining and predicting the bubble diameter.

Mapping of the dimensionless bubble diameter with applied voltage and liquid physical parameters

In Fig. 7, the non-dimensional bubble diameter (D_b/D_{ch}) is plotted as a function of the applied voltage for four solutions of different concentration of glycerol. It can be seen that in all cases the non-dimensional bubble diameter decreases with increasing voltage, while it reaches a plateau at voltages higher than ~12 kV. When low voltage is applied, the electric field assists with the compression of the neck of the dispersed

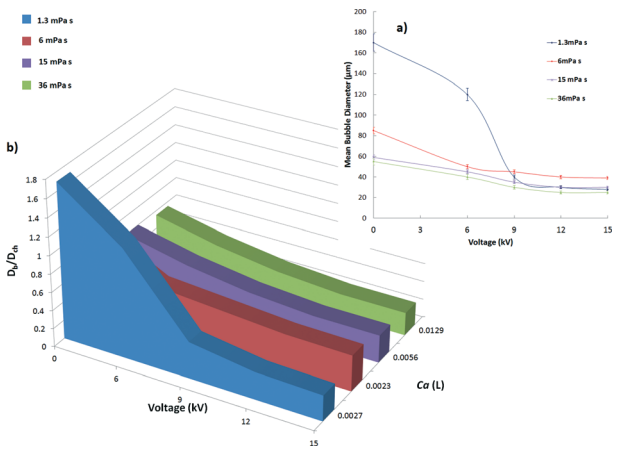

Fig. 5 a) Graph showing variation of bubble diameter with applied voltage for solution viscosities of 1.3, 6, 15 and 36 mPa s, and b) 3D plot of dimensionless bubble diameter with respect to voltage and capillary number increment. Error bars in Fig. 5a refer to repeat experiments.

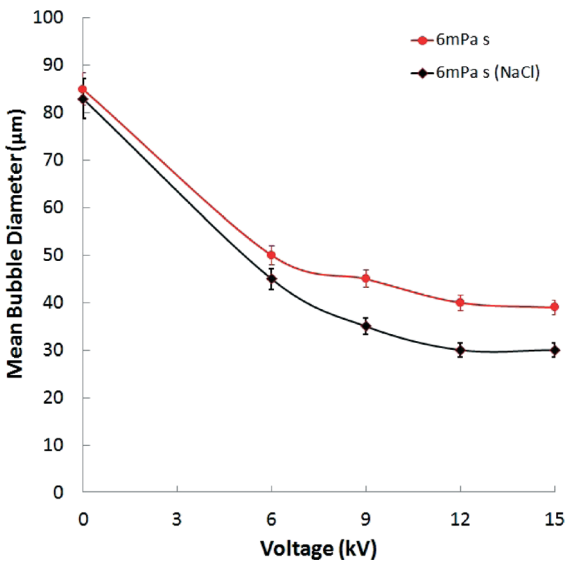

Fig. 6 Graph showing variation of mean bubble diameter with applied voltage for solution with constant viscosity of 6 mPa s with and without the addition of 1 wt.% NaCl solution (PDI < 1%). Error bars refer to repeat experiments.

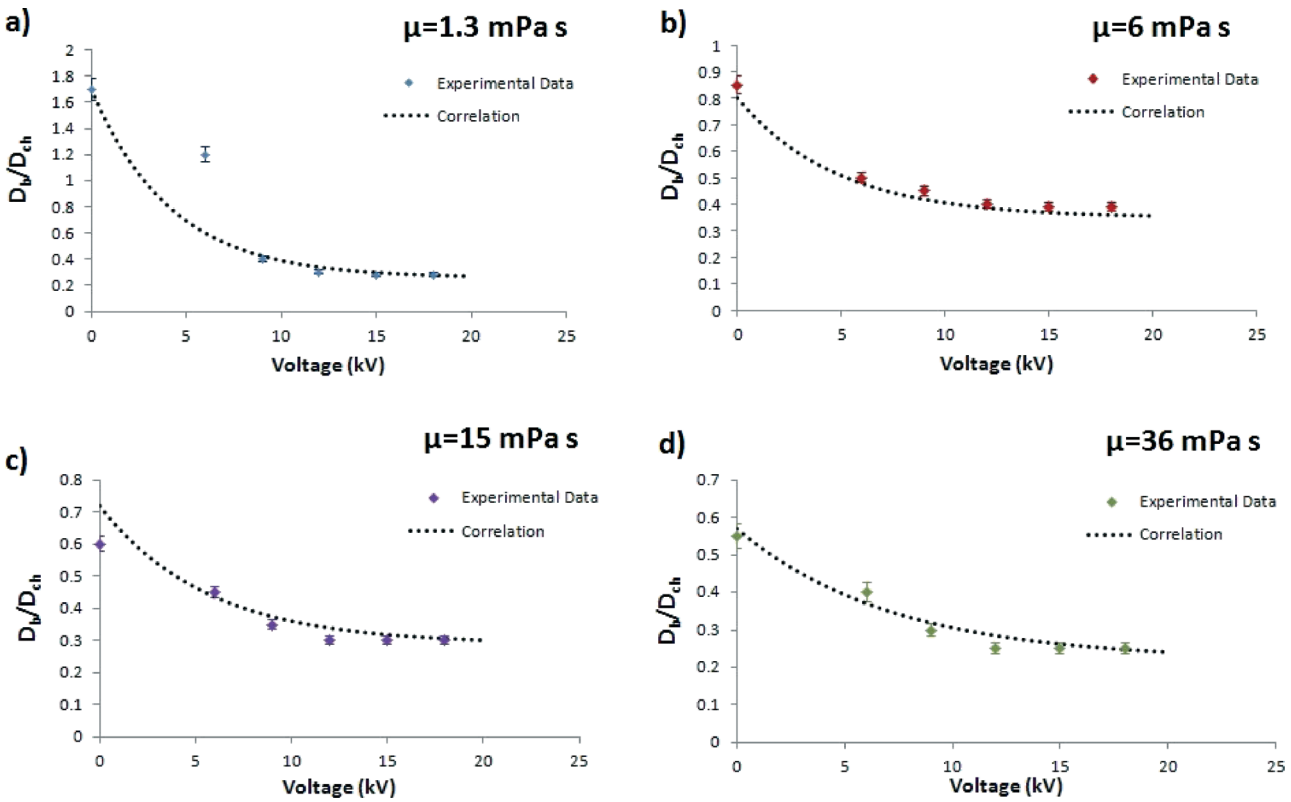

Fig. 7 Variation in bubble dimensionless diameter for solutions with a viscosity of a) 1.3, b) 6,) c) 15 and d) 36 mPa s. (PDI < 1%).

phase, resulting in an approximately linear decrease in bubble size for voltages ≤12 kV.

By further increasing the applied voltage, the width of the neck during the breakup reduces. However, similar to observations reported by Kim *et al.*[38] jetting occurs and there is very little further effect on the bubble size. The production of monodisperse bubbles was found to cease at voltages more than 20 kV. For each case, an asymptotic curve is fitted to show this limit in the reduction of bubble size. It can also be seen that the solutions of higher concentration of glycerol (*i.e.* higher viscosity) follow a similar trend, whilst in the case for the solution with the lowest viscosity the trend is slightly changed due to the fact that the electrical conductivity is comparatively lower. For the range of Ca numbers investigated, a general predictive model is obtained where the normalized bubble diameter can be estimated as the following:

$$\frac{D_b}{D_{ch}} = (-11.8\mathrm{Ca} + 0.37) + (-0.98\mathrm{Ca} + 0.5)e^{(6.8\mathrm{Ca}-0.2)V} \quad (6)$$

This model can predict the dimensionless bubble size for a range of capillary numbers 0.001 ≤ Ca ≤ 0.04, with approximately 8% error. In Fig. 8, the experimental values for D_b/D_{ch} are plotted against the predicted values and the proximity of the experimental data to the parity line suggests that the predictive model is in agreement with the experimental data especially for the obtained values of $D_b/D_{ch} < 0.6$. This model does not take into account the geometrical aspects of the channel (*i.e.* the gap between the capillaries), as these parameters also affect the bubble size.

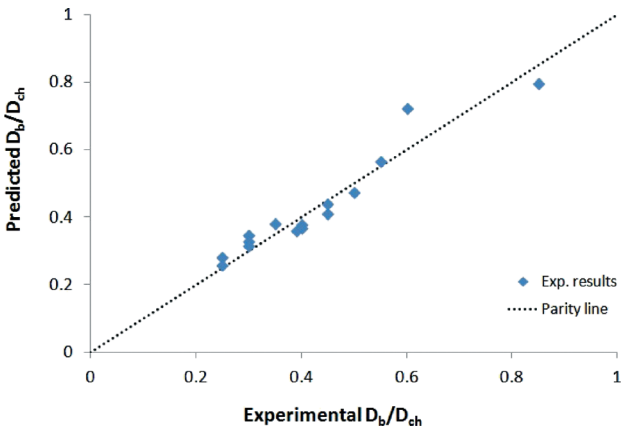

Fig. 8 Graph representing experimental data for dimensionless bubble diameter against predicted values.

Influence of electric field on bubble uniformity and production rate

Microbubbles produced with an applied voltage ≤15 kV were highly monodisperse (polydispersity index ≤ 1%). It was found that the applied electric field only increased the velocity of the suspension flow and had little effect on the uniformity of the bubbles produced.

Fig. 9 depicts the number of bubbles produced with and without the presence of an electric field for different solution viscosities over a fixed time period of 5 s and collection area of 1.5 mm^2. It is shown that by increasing the voltage not only did the bubbles become smaller but also the production rate increased. In addition, from the data obtained from the high speed camera images, for a given liquid flow rate of 0.01 ml min^{-1}, the number of bubbles in every 1 ml of the collected sample is between 2×10^6 and 6×10^6 depending on the bubble size.

Comparison with other bubble formation techniques

Three of the most commonly used methods of producing microbubbles are sonication, electrohydrodynamic (EHD) bubbling and microfluidics.[1] Amongst these techniques, sonication produces microbubbles with diameters smaller than 10 μm with a very wide size distribution (PDI > 30%). While the production rate is very high with the sonication method, it is also limited by being a batch technique. The number of microbubbles formed per unit using the EHD technique proposed by Farook *et al.*[3] is smaller than that obtained using the sonication method but it is continuous and relatively immune to nozzle clogging. To date, however the polydispersity indices obtained are inferior to those reported with microfluidics (PDI < 2%). One of the main problems with microfluidics is that in order to produce microbubbles suitable for biomedical applications, it is necessary to use microchannels with diameters <10 μm which are easily blocked by material residue. Also it is very difficult to pump highly viscous liquid through these channels due to the higher pressure drop so that production rates are low. Hettiarachchi *et al.*[39] showed that bubbles could be generated in a jetting mode rather than bubble dripping mode in a microfluidic device. They used high flow rates and gas pressures (*i.e.* $Q_l > 1$ μl s^{-1} $P_g > 10$ psi) to increase the production rate, but due to the relative instability of this mode and increased risk of bubble coalescence, the polydispersity of the microbubbles formed was >50%. Furthermore, Kendall *et al.*[40] used a multi array microfluidic flow focusing geometry containing up to eight channels to scale up the production of bubbles. They have reported the highest production at 1.34×10^5 Hz (bubbles per second) with bubble size ranging between 18.6–22.3 μm and polydispersity index <9%. In the present study bubbles were produced at a rate of ~10^3 Hz due to the much lower liquid flow rates compared to the studies mentioned above. The polydispersity index was however maintained at <1% and the ratio of bubble to capillary size much smaller, thereby reducing the risk of clogging. The technique could be employed in a multi-channel format to increase production rate but this was not the focus of this work.

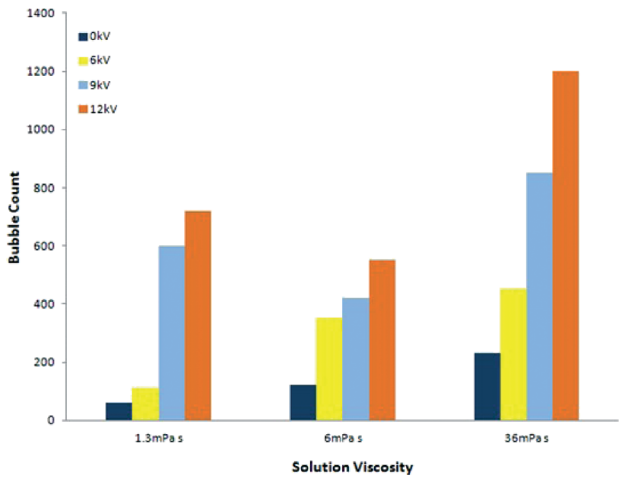

Fig. 9 Graph showing variation in the number of bubbles generated with applied voltage for three different solution viscosities of 1.3, 6 and 36 mPa s over a fixed time period of 5 seconds and collection area of 1.5 mm^2.

A key question is whether or not the bubble size can be further reduced using this technique to enable production of microbubbles with diameters <10 μm (such as would be required for intravenous administration in biomedical applications). The most obvious means of achieving this would be to use a device with smaller capillaries. If similar ratios of bubble: capillary diameter could be achieved as shown in Fig. 7 then using capillaries of half the size (50 μm internal diameter) would yield microbubbles in the desired range, whilst still giving greatly reduced risk of clogging compared with existing devices in which the bubble : channel diameter ratio is ~1. This raises the further question as to whether or not a proportional reduction in bubble size can be achieved in smaller capillaries with the application of an electric field. Eqn (2) indicates that the electrophoretic force decreases with bubble volume whilst eqn (3) shows that the capillary force scales approximately with radius. Eqn (4) and (5) indicate that the viscous and pressure forces scale with projected area but also with liquid volume flow rate and gas pressure respectively. The effect on bubble size will therefore depend upon the relative change in these latter two quantities. Previous work by the authors[26] has shown that the rate at which bubble size decreases with the ratio of liquid to gas flow rates increases with decreasing capillary size. This would suggest that even with a reduction in the relative influence of F_{DEP} it would still be possible to generate microbubbles substantially smaller than the capillary. Future work will aim to demonstrate this.

There are numerous applications from biomedical imaging to food and water treatment that require microbubbles with a controlled range of sizes. For instance, microbubble induced cavitation has been proposed as an innovative method for minimally-invasive drug delivery.[10] Microbubble assisted flotation is widely used in the recovery of fine mineral particles and flotation and for solid–liquid separation to remove pollutants. Recent bench studies of flotation of different minerals; with injection of microbubbles (40 μm, mean diameter) to lab cells (in addition to the cell generated coarse bubbles) have significantly improved separation efficiency when compared to the mill standard.[41] Microbubbles

have been shown to increase fermentation rates in the production of biofuels whilst mixtures of ozone nanobubbles with oxygen microbubbles have been shown to be more effective in fighting bacteria than conventional ozone saturated water.[42] Each of these applications required the concentration, size and size distribution of microbubbles to be tightly controlled in order to maximise efficacy. Many of the key characteristics of microbubbles are directly related to their size (*e.g.* stability, buoyancy and surface activity) and in this work we have presented a new technique for microbubble formation which offers excellent control over bubble size and polydispersity, continuous production with lower risk of clogging and the potential for multiplexing to achieve higher production rates. However, in order to be useful in biomedical applications, the size of the microbubbles need to be further reduced to <10 μm and this is being addressed in our current work as indicated above.

Conclusions

Monodisperse microbubbles were successfully produced using an integrated microfluidic and electrohydrodynamic device. A systematic investigation of bubble formation at different applied voltages and with different liquid properties was performed. It was shown that bubbles with diameters much smaller than that of the microchannel could be produced with a polydispersity index ~1%. A critical voltage of 12 kV was determined above which no further reduction in bubble size was achieved, and this limit was not affected by increasing the solution viscosity or electrical conductivity within the ranges used in this study. The observed dependence of bubble size on applied voltage is consistent with electrohydrodynamic theory. In addition to reducing the bubble size, applying an electrical potential difference increased the rate at which bubbles were produced.

Acknowledgements

The authors wish to thank the Engineering and Physical Science Research Council, UK for providing the Phantom V7.1 high speed camera for this work. The generous help of Adrian Walker of the Instrument Loan Pool is gratefully acknowledged.

Notes and references

1 E. Stride and M. Edirisinghe, *Soft Matter*, 2008, **4**, 2350–2359.
2 Y. Cui and P. A. Campbell, *2008 IEEE Ultrasonics Symposium*, 2008, pp. 1663–1666.
3 U. Farook, E. Stride, M. J. Edirisinghe and R. Moaleji, *Med. Biol. Eng. Comput.*, 2007, **45**, 781–789.
4 P. Garstecki, I. Gitlin, W. DiLuzio, G. M. Whitesides, E. Kumacheva and H. A. Stone, *Appl. Phys. Lett.*, 2004, **85**, 2649–2651.
5 K. Hettiarachchi, E. Talu, M. L. Longo, P. A. Dayton and A. P. Lee, *Lab Chip*, 2007, **7**, 463–468.
6 C. Chen, Y. Zhu, P. W. Leech and R. Manasseh, *Appl. Phys. Lett.*, 2009, **95**, 144101.
7 M. De Menech, P. Garstecki, F. Jousse and H. A. Stone, *J. Fluid Mech.*, 2008, **595**, 141–161.
8 S.-Y. Teh, R. Lin, L.-H. Hung and A. P. Lee, *Lab Chip*, 2008, **8**, 198–220.
9 U. Farook, E. Stride and M. Edirisinghe, *J. R. Soc., Interface*, 2009, **6**, 271–277.
10 K. Ferrara, R. Pollard and M. Borden, *Annu. Rev. Biomed. Eng.*, 2007, **9**, 415–447.
11 S. Hernot and A. L. Klibanov, *Adv. Drug Delivery Rev.*, 2008, **60**, 1153–1166.
12 J. R. Anderson, D. T. Chiu, H. Wu, O. J. Schueller and G. M. Whitesides, *Electrophoresis*, 2000, **21**, 27–40.
13 H. M. Wyss, D. L. Blair, J. F. Morris, H. A. Stone and D. A. Weitz, *Phys. Rev. E: Stat., Nonlinear, Soft Matter Phys.*, 2006, **74**, 061402.
14 J. Chakraborty, S. Ray and S. Chakraborty, *Electrophoresis*, 2012, **33**, 419–425.
15 T. Bayraktar and S. B. Pidugu, *Int. J. Heat Mass Transfer*, 2006, **49**, 815–824.
16 I. Glasgow, J. Batton and N. Aubry, *Lab Chip*, 2004, **4**, 558–562.
17 J. Zeng, *Int. J. Mol. Sci.*, 2011, **12**, 1633–1649.
18 J. S. H. Lee and D. Li, *Microfluid. Nanofluid.*, 2006, **2**, 361–365.
19 V. Reddy and J. D. Zahn, *ASME Int. Mech. Eng. Expo. Conf., Proc.*, 2005, 267–276.
20 S. J. Kim, Y.-A. Song, P. L. Skipper and J. Han, *Anal. Chem.*, 2006, **78**, 8011–8019.
21 A. Ahmadi, J. F. Holzman, H. Najjaran and M. Hoorfar, *Microfluid. Nanofluid.*, 2011, **10**, 295–305.
22 A. K. Sen, J. Darabi and D. R. Knapp, *J. Fluids Eng.*, 2011, **133**, 071301.
23 B. Ahmad, O. Gunduz, S. Stoyanov, E. Pelan, E. Stride and M. Edirisinghe, *Carbohydr. Polym.*, 2012, **89**, 222–229.
24 Y. Srivastava, I. Loscertales, M. Marquez and T. Thorsen, *Microfluid. Nanofluid.*, 2008, **4**, 245–250.
25 K. Pancholi, E. Stride and M. Edirisinghe, *J. Drug Targeting*, 2008, **16**, 494–501.
26 M. Parhizkar, M. Edirisinghe and E. Stride, *Microfluid. Nanofluid.*, 2013, **14**, 797–808.
27 W. Kim, J. C. Ryu, Y. K. Suh and K. H. Kang, *Appl. Phys. Lett.*, 2011, **99**, 224102.
28 F. Chen, Y. Peng, Y. Z. Song and M. Chen, *Exp. Therm. Fluid Sci.*, 2007, **32**, 174–181.
29 X. Quan, G. Chen and P. Cheng, *Int. J. Heat Mass Transfer*, 2011, **54**, 2110–2115.
30 S. D. Oh and H. Y. Kwak, *Heat Transfer Eng.*, 2000, **21**, 33–45.
31 P. Garstecki, M. J. Fuerstman, H. A. Stone and G. M. Whitesides, *Lab Chip*, 2006, **6**, 437–446.
32 G. F. Christopher, N. N. Noharuddin, J. A. Taylor and S. L. Anna, *Phys. Rev. E: Stat., Nonlinear, Soft Matter Phys.*, 2008, **78**, 036317.
33 G. Taylor, *Proc. R. Soc. London Ser. A*, 1964, **280**, 383–390.
34 S. N. Jayasinghe and M. J. Edirisinghe, *J. Nanosci. Nanotechnol.*, 2005, **5**, 923–926.

35 R. Behrends, K. Fuchs, U. Kaatze, Y. Hayashi and Y. Feldman, *J. Chem. Phys.*, 2006, **124**, 144512.
36 C. Pantano, A. M. Gañán-Calvo and A. Barrero, *J. Aerosol Sci.*, 1994, **25**, 1065–1077.
37 B. K. Ku and S. S. Kim, *J. Aerosol Sci.*, 2002, **33**, 1361–1378.
38 H. Kim, D. Luo, D. Link, D. A. Weitz, M. Marquez and Z. Cheng, *Appl. Phys. Lett.*, 2007, **91**, 113106.
39 K. Hettiarachchi, E. Talu, M. L. Longo, P. A. Dayton and A. P. Lee, *Lab Chip*, 2007, **7**, 463–468.
40 M. R. Kendall, D. Bardin, R. Shih, P. A. Dayton and A. P. Lee, *Bubble Sci., Eng., Technol.*, 2012, **4**, 12–20.
41 T. Yalcin, A. Byers and K. Ughadpaga, *Miner. Process. Extr. Metall. Rev.*, 2002, **23**, 181–197.
42 M. Kukizaki and M. Goto, *J. Membr. Sci.*, 2006, **281**, 386–396.